Coupled polarization and acoustic-phonon dynamics after optical excitation of quantum dots near surfaces

B. Krummheuer,* V. M. Axt, and T. Kuhn
Institut für Festkörpertheorie, Westfälische Wilhelms-Universität, Wilhelm-Klemm-Str. 10, 48149 Münster, Germany
(Received 30 June 2005; revised manuscript received 31 October 2005; published 29 December 2005)

An analysis of the pure dephasing of a single quantum dot embedded in a half-space or a free-standing slab due to the interaction of the carriers with confined acoustic phonons is presented. We discuss the time dependence of the polarization and the relative volume change based on exact expressions which hold for ultrafast excitation. We find that the proximity of the quantum dot to a surface leaves distinct traces in the polarization and in the case of the half-space leads to an additional decay. In the case of the slab the polarization shows a pronounced periodic structure depending on the width of the slab.

DOI: 10.1103/PhysRevB.72.245336 PACS number(s): 73.21.La, 63.20.Kr, 63.22.+m, 78.47.+p

I. INTRODUCTION

In the past years semiconductor quantum dots (QDs) have become the basis for several optoelectronic applications, like lasers[1] or single photon sources[2] and they are discussed as building blocks for quantum information devices.[3] In most modern frabrication techniques the QDs are grown within layered structures and are usually located near interfaces or surfaces. In order to obtain a thorough understanding of the optical properties of QDs it is therefore of great interest to study how they are influenced by the proximity to a surface.

One of the properties that is expected to differ significantly from the behavior far away from surfaces is the carrier-phonon interaction, since the phonon modes in confined structures are quite unlike those in an infinite bulk. The reason for this is the reflection of phonons at the surfaces which features a partial mode conversion between longitudinal and transverse phonons as well as the existence of surface phonons.

Based on the classical treatment of confined acoustic waves[4,5] the quantum mechanical study of confined phonon modes has become well established.[6] With the growing technological importance of semiconductor heterostructures this field has been extended to focus on the implications these phonons have for the description of quantum wells, wires and dots.[7–11] In the past the influence of confined optical phonons has been studied intensely,[12–16] because optical phonons often provide a dominant channel for energy relaxation of electrons in low dimensional structures. But also the interest in acoustic phonons has grown. While some of these studies have investigated the acoustic phonon modes in half-space geometries,[17,18] others have concentrated on so called free-standing structures surrounded by vacuum[19–25] or nanostructures embedded in another material.[25] Today, such free-standing structures are far from presenting only a theoretical model, but can be manufactured and characterized[26,27] and they are promising candidates for nanoelectromechanical applications.

Most works restricted themselves to a semiclassical description of the carrier-confined phonon interaction, i.e., the calculation of scattering rates from Fermi's golden rule. However, it has been shown[28–30] that in particular in QD structures at low temperatures and for small dot sizes the carrier dynamics and phonon dynamics are mainly governed by processes which cannot be described within a Markov approximation and therefore require a full quantum kinetic approach. These processes, often referred to as pure dephasing, will be studied in this paper.

We will concentrate on the influence of confined phonon modes on the decay of the optical polarization of a QD embedded in a half-space or a free-standing slab after the excitation with a short laser pulse. The excitation of a QD with an ultrashort laser pulse leads to the buildup of a phonon occupation within the QD. Part of this occupation remains within the QD and forms a stable polaron, while the other part carries away the surplus energy in form of a phonon wave packet traveling outward with sound velocity.[31] This wave packet is responsible for the irreversible decay of the polarization. In the presence of a surface it is to be expected that it is reflected and reenters the QD. In this paper we want to study, how the coherence of the quantum dot system is influenced by this reencounter of the phonon wave packet. Since for many materials such as GaAs typically the main contribution to the carrier-phonon interaction in a QD is given by the coupling via deformation potential to acoustic phonons we will restrict ourselves to this interaction mechanism. Other coupling mechanisms like the coupling to piezoelectric and polar optical coupling may become relevant in strongly polar materials such as GaN (Ref. 32) and are straight forward to include when needed.

The paper is organized as follows. In Sec. II we present the theory necessary for our study. First, we briefly discuss the general theoretical description of phonons in confined structures. In the Secs. II A and II B we specialize the discussion to phonon modes in a half-space and a slab. A short section on the pure dephasing in QDs (Sec. II C) completes the theoretical part. We then discuss the results of numerical simulations in Sec. III, first for the half-space and then for the slab and end with our conclusions in Sec. IV. The Appendix shows the detailed expressions for the electron-phonon coupling matrix elements of the various phonon modes.

II. THEORY

Phonon modes in confined structures differ strongly from those in an infinite bulk system. In confined structures longitudinal and transverse phonons are coupled via the boundary conditions even in isotropic media unlike in the case of electromagnetic waves.[5] When acoustic phonons impinge on a surface, there is in general a partial conversion between longitudinal and transverse phonons. This leads to phonon modes, which cannot strictly be classified as longitudinal or transverse.

Another effect that must be accounted for when surfaces are involved is the existence of so-called surface phonons. Unlike for the bulklike modes the displacement field associated with surface phonons is concentrated in the close proximity of the surface. The amplitude decreases exponentially with increasing distance from the surface. The bulklike modes therefore present standing waves in the direction of confinement, while the surface modes are evanescent. Bulklike and surface modes do, however, still not form a complete set of eigenmodes of the lattice. Rather, a third type of modes must be taken into account which we will denote as *mixed modes*, because they show the typical behavior of surface modes in their longitudinal component and the behavior of bulklike modes in their transverse component.

The starting point for the derivation of phonon modes is the wave equation for the displacement field which, for freestanding interfaces, has to be complemented by the boundary condition of a stress-free surface.[33,34] This yields a set of modes which are characterized by a complete set of quantum numbers ξ. The quantum numbers chosen here are $\xi=(\mathbf{q}_\parallel, q_l, m)$, where m stands for the different phonon types described in detail in the following, $\mathbf{q}_\parallel$ is the wave vector in the plane parallel to the surface, and q_l is the z component of the wave vector of the longitudinal part of the mode. The quantization of the complete elastic displacement field $\mathbf{u}(\mathbf{r},t)$ is then given by

$$\mathbf{u}(\mathbf{r},t)=\sum_\xi \sqrt{\frac{\hbar}{2\varrho\omega_\xi}} b_\xi \frac{1}{2\pi} e^{i\mathbf{q}_\parallel \mathbf{r}_\parallel} \mathbf{u}_\xi(z) + h.c., \tag{1}$$

where *h.c.* denotes the hermitian conjugate, $\mathbf{u}_\xi(z)$ is the displacement mode function and $b_\xi(b_\xi^\dagger)$ stands for the destruction (creation) operator for a phonon of the mode ξ. The sum in the above expression is of symbolic nature, it stands for a summation over the discrete modes and an integration over the continuous modes.

The different phonon types can be classified in terms of their dispersion ω_ξ. However, it is sometimes more instructive to do so with regard to their surface velocity $c_s=\omega_\xi/q_\parallel$. The surface modes, which are often called Rayleigh waves, have surface velocities smaller than the transverse sound velocity c_t. The bulklike modes are characterized by surface velocities larger than the longitudinal sound velocity c_l, while the modes with a mixed surface and bulklike character have surface velocities in the range $c_t<c_s<c_l$. For the purely transverse modes the surface velocities are larger than the transverse sound velocity: $c_s>c_t$.

For the deformation potential coupling of carriers and phonons the interaction is mediated by a potential, which is proportional to the relative volume change $\delta V/V$ associated with longitudinal phonons. This interaction potential $v_{c\text{-}ph}$ can be expressed as[35]

$$v_{c\text{-}ph}(\mathbf{r})=D^c\frac{\delta V}{V}=D^c \mathrm{div}\, \mathbf{u}(\mathbf{r},t), \tag{2}$$

where D^c stands for the deformation potential of the conduction ($c=e$) or the valence ($c=h$) band. The carrier-phonon Hamiltonian in second quantization can then be expressed in terms of the phonon displacement field and the field operators for the carriers ψ and $\psi^\dagger$

$$H_{c\text{-}ph}=\int d^3r \psi^\dagger(\mathbf{r}) v_{c\text{-}ph}(\mathbf{r}) \psi(\mathbf{r}). \tag{3}$$

In this paper we model the QD as a two level system with an upper level for the electron and a lower level for the hole. For small QDs, in which further levels are energetically far away, this is a good approximation. The field operator can then be written as

$$\psi(\mathbf{r})=\varphi^e(\mathbf{r})c+\varphi^h(\mathbf{r})d^\dagger, \tag{4}$$

where $c^\dagger$ and c ($d^\dagger$ and d) represent the creation and destruction operators for an electron (hole) in the lowest (uppermost) conduction- (valence-) band state and $\varphi^e(\mathbf{r})[\varphi^h(\mathbf{r})]$ is the electron (hole) wave function. Since the interband coupling due to phonons is negligible, one obtains the following expression for the interaction Hamiltonian

$$H_{c\text{-}ph}=\hbar\sum_\xi (g_\xi^e b_\xi c^\dagger c - g_\xi^h b_\xi d^\dagger d + h.c.). \tag{5}$$

The electron (hole-) phonon coupling matrix element is represented by $g_\xi^e(g_\xi^h)$. The form of the coupling matrix element depends strongly on the confined phonon mode involved as will be discussed in the following sections and in the Appendix. In any case the coupling matrix element always factorizes into two parts

$$g_\xi^c=\mathcal{G}_\xi^c\mathcal{F}_\xi^c \tag{6}$$

with $c\in\{e,h\}$. The first part $\mathcal{G}_\xi^c$ stands for the coupling matrix elements of bulklike electron and hole states. In the second part, the form factor $\mathcal{F}_\xi^c$, the confined carrier wave functions enter and it therefore accounts for the carrier confinement. For a QD in an infinite system these functions read

$$\mathcal{G}_\xi^c=D^c\sqrt{\frac{1}{2\varrho\hbar\omega_\xi(2\pi)^3}}q \tag{7}$$

and

$$\mathcal{F}_\xi^c=\int |\varphi^c(\mathbf{r})|^2 e^{i\mathbf{q}\mathbf{r}} d^3r \tag{8}$$

with $q=|\mathbf{q}|$ and $\varphi^c(\mathbf{r})$ is the carrier wave function. In the cases of a half-space and a slab, which are the subject of the present paper, both functions will be modified. The explicit expressions for the various modes will be given in the Appendix.

A. Phonons in a half-space

The phonon modes in a half-space have been previously analyzed in Ref. 6, where also a proof for their orthonormality and completeness is given. Here, however, unlike in Ref. 6 we choose q_l as the second quantum number for all modes involving a longitudinal component, since this component couples to the carrier system. In addition this is the natural quantum number for unconfined longitudinal phonons. Thus our results can be more readily compared with those obtained in an infinite bulk system. Our modes are therefore orthonormalized with respect to q_l, so that the normalization constants are different from those in Ref. 6. In a half-space there are purely transverse phonons and others, which are a mixture of transverse and longitudinal ones. Since for the following analysis of the carrier-phonon coupling via deformation potential the purely transverse modes are of no importance, they will not be considered here.

The two orthogonal modes with $c_s > c_l$ are denoted by different names in the literature. In seismography they are usually called the mixed P-SV modes. Following the nomenclature of the phonon modes in a slab, we will refer to them as the dilatational and the flexural modes. These names become clearer if first taking a look at the slab case. In the slab the dilatational modes displace the two surfaces with a phase shift of π causing contractions and expansions of the slab width. For the flexural modes the surfaces are displaced in phase, so that the wave bends the slab without changing its width. In the case of the flexural modes of the half-space the divergence of the displacement field, which describes the relative volume change, vanishes at the surface, i.e., at $z=0$. The dispersion relation for these modes is given by

$$\omega^2_{q_\parallel,q_l,\mathrm{dil}} = \omega^2_{q_\parallel,q_t,\mathrm{flex}} = c_l^2(q_\parallel^2 + q_l^2) = c_t^2(q_\parallel^2 + q_t^2), \tag{9}$$

where q_t is the z component of the wave vector of the transverse part of the mode.

For the mixed modes with $c_l > c_s > c_t$ the dispersion relation reads $\omega^2_{q_\parallel,q_l,\mathrm{mix}} = c_l^2(q_\parallel^2 - q_l^2) = c_t^2(q_\parallel^2 + q_t^2)$. With regard to q_l these modes resemble evanescent surface modes while with regard to q_t they have the properties of standing bulklike modes.

The surface or Rayleigh modes are the only phonon modes in the half-space which are discrete with respect to q_l. This means that not all q_l are allowed. The possible values for q_l depend on the sound velocities of the material concerned[6] and for GaAs one finds $q_l = 0.81 q_\parallel$ and $\omega_{q_\parallel,q_l,\mathrm{sur}} = c_l^2(q_\parallel^2 - q_l^2) = c_t^2(q_\parallel^2 - q_t^2)$, so that the surface velocity is smaller than c_t.

The deformation potential coupling matrix elements for these modes are given in Appendix A.

B. Phonons in a slab

Let us now consider the case of a slab with two boundaries at $z = \pm d/2$. The phonon modes in such a slab are calculated in Ref. 4, and are also given in Refs. 21 and 33. For the slab the different phonon modes can be written in a more compact form than in the half-space if q_l and q_t are permitted to be either real or purely imaginary and if the following three combinations are possible: q_l, q_t are both real, q_l, q_t are both purely imaginary, or q_t is real and q_l purely imaginary. The relation in Eq. (9) thus describes all three former cases and can yield modes with surface velocity c_s larger than c_l, between c_l and c_t, and smaller than c_t. As in the half-space the full set of quantum numbers needed to describe the modes is $\xi = (\mathbf{q}_\parallel, q_l, m)$. However, unlike in the half-space q_l and q_t are now always discrete. For the dilatational modes the possible values for q_l and q_t are determined by the equations

$$\frac{\tan q_t d/2}{\tan q_l d/2} = -\frac{4q_\parallel^2 q_l q_t}{(q_\parallel^2 - q_t^2)^2}, \tag{10}$$

while for the flexural modes we have

$$\frac{\tan q_t d/2}{\tan q_l d/2} = -\frac{4q_\parallel^2 q_l q_t}{(q_\parallel^2 - q_t^2)^2}. \tag{11}$$

Because of the possible imaginary value of the q_z components the modes can be written in a very compact form, which includes the bulklike modes, the surface modes, and those with mixed character all in two expressions. The coupling matrix elements for the case of slab geometry are given in Appendix B.

C. Dephasing

In this paper we want to analyze the influence of confined phonons on the optical properties of a QD. Specifically, we are interested in the dephasing of the optical polarization through the interaction of carriers with confined phonons and the resulting phonon dynamics.

It is known, that for low temperatures and small QDs the main contribution to the loss of coherence is given by the process of pure dephasing.[28–30] To study the light-induced dynamics the system described above has to be complemented by the usual dipole coupling to the light field. For the case of excitation by a δ-like laser pulse of arbitrary strength the polarization can be calculated exactly. It is given by[31]

$$\mathbf{P}(t) = \mathbf{M}_0^* \langle dc \rangle = \mathbf{M}_0^* p(t) = \theta(t) \frac{i\mathbf{M}_0^* \sin(f)}{2} e^{-i\bar{\Omega}t} e^{-i\sum_\xi |\gamma_\xi|^2 \sin(\omega_\xi t)} \times \exp\left[-\sum_\xi |\gamma_\xi|^2 [1 - \cos(\omega_\xi t)][1 + 2n_\xi] \right], \tag{12}$$

where

$$n_\xi := \frac{1}{e^{\frac{\hbar\omega_\xi}{k_B T}} - 1} \tag{13}$$

denotes the equilibrium phonon occupation at temperature T and $\gamma_\xi := g_\xi / \omega_\xi$ is a dimensionless coupling strength, where $g_\xi := g_\xi^e - g_\xi^h$. The polaron shifted gap energy is given by $\bar{\Omega} := \Omega - \Sigma_\xi \omega_\xi |\gamma_\xi|^2$ and f is the pulse area. Note, that this expression for the polarization is exact with regard to the carrier-light and carrier-phonon interaction. It should also be added, that the limit of ultrashort pulses is reached for pulses which are shorter than the characteristic time scale for carrier-phonon interaction processes. For typical QDs this is

fulfilled for pulses shorter than a few hundred femtoseconds.[30]

The excitation of a QD with an ultrashort pulse leads to the creation of phonons. Since for the coupling via deformation potential only the longitudinal phonons are important, it is instructive to look at the relative volume change connected with these phonons.[36] The relative volume change is given by

$$\frac{\delta V}{V} = \mathrm{div}\,\mathbf{u}(\mathbf{r},t) = \frac{1}{2\pi}\sum_{\xi} S_{\xi} R_{q_l,m}(z)(b_{\xi} e^{i\mathbf{q}_{\parallel}\mathbf{r}_{\parallel}} + b_{\xi}^{\dagger} e^{-i\mathbf{q}_{\parallel}\mathbf{r}_{\parallel}}), \tag{14}$$

with $S_{\xi}=\mathcal{G}_{\xi}^{c}/D^{c}$ and

$$R_{q_l,m}(z) = \begin{cases} \cos q_l z, & \text{if } m = \text{dil} \\ \sin q_l z, & \text{if } m = \text{flex} \\ e^{-q_l z}, & \text{if } m = \text{mix or } m = \text{sur} \end{cases} \tag{15}$$

for the half-space and

$$R_{q_l,m}(z) = \begin{cases} \cos q_l z, & \text{if } m = \text{dil} \\ \sin q_l z, & \text{if } m = \text{flex} \end{cases} \tag{16}$$

for the slab. With the exact result[31,36]

$$\langle b_{\xi} \rangle = \sin^2\left(\frac{f}{2}\right)\gamma_{\xi}^{*}(e^{-i\omega_{\xi}t} - 1) \tag{17}$$

one then finds for the expectation value

$$\left\langle \frac{\delta V}{V} \right\rangle = \frac{1}{\pi}\sin^2\left(\frac{f}{2}\right)\mathrm{Re}\left[\sum_{\xi} S_{\xi} R_{q_l,m}(z)\,\gamma_{\xi}^{*}(e^{-i\omega_{\xi}t} - 1)e^{i\mathbf{q}_{\parallel}\mathbf{r}_{\parallel}}\right], \tag{18}$$

where Re{…} denotes the real part. In Ref. 31 it has been shown analytically that for acoustic phonons in a bulk system this function corresponds to an outgoing spherical wave packet and a part which remains in the dot region. In the present case, where the phonon modes are more complicated this cannot be seen so easily. However, we will see from the numerical evaluation in Sec. III that also here we have these two parts.

The relative volume change is a very intuitive variable. It describes the change of the potential which mediates the carrier-phonon interaction. However, this change does not fully represent the variable which couples back to the induced polarization. In particular, the volume change is not responsible for its dephasing. In the following we will therefore introduce a *complex volume change*. Its real part corresponds to the relative volume change and leads to a frequency shift of the polarization, thus describing the polaron created by the carrier-phonon interaction. The imaginary part induces the dephasing.

With the help of the equation for the field-free evolution that follows the ultrafast laser action the change of the polarization can be described by

$$\frac{d}{dt}\langle dc\rangle = -i\Omega\langle dc\rangle - \frac{i}{\hbar}\int d^3r(D^e|\varphi_e|^2 - D^h|\varphi_h|^2)\left\langle dc\frac{\delta V}{V}\right\rangle, \tag{19}$$

with

$$\left\langle dc\frac{\delta V}{V}\right\rangle = \frac{1}{2\pi}\sum_{\xi} S_{\xi} R_{q_l,m}(z)(\langle b_{\xi} dc\rangle e^{i\mathbf{q}_{\parallel}\mathbf{r}_{\parallel}} + \langle b_{\xi}^{\dagger} dc\rangle e^{-i\mathbf{q}_{\parallel}\mathbf{r}_{\parallel}}). \tag{20}$$

Using again the exact solution for the ultrashort pulse excitation,[31] we obtain

$$\left\langle dc\frac{\delta V}{V}\right\rangle = \frac{p(t)}{2\pi}\sum_{\xi} S_{\xi} R_{q_l,m}(z)[-\gamma_{\xi}(e^{i\omega_{\xi}t} - 1)n_{\xi}e^{-i\mathbf{q}_{\parallel}\mathbf{r}_{\parallel}} + \gamma_{\xi}^{*}(e^{-i\omega_{\xi}t} - 1)(1 + n_{\xi})e^{i\mathbf{q}_{\parallel}\mathbf{r}_{\parallel}}] =: p(t)y(\mathbf{r},t). \tag{21}$$

It is interesting to see, that now the equation of motion for the polarization can be written as

$$\frac{d}{dt}p(t) = -i\Omega p(t) - \frac{i}{\hbar}Y(t)p(t), \tag{22}$$

where

$$Y(t) = \int (D^e|\varphi^e(\mathbf{r})|^2 - D^h|\varphi^h(\mathbf{r})|^2)y(\mathbf{r},t)d^3r. \tag{23}$$

One thus finds for the square modulus of the polarization

$$\frac{d}{dt}|p(t)|^2 = \frac{2}{\hbar}\mathrm{Im}\{Y(t)\}|p(t)|^2. \tag{24}$$

Im{…} denoting the imaginary part. Since in this paper we concentrate on the behavior of the polarization at very low temperatures, we have in the limiting case $T=0$ K:

$$y(\mathbf{r},t)_{T=0} = \frac{1}{2\pi}\sum_{\xi} S_{\xi} R_{q_l,m}(z)\,\gamma_{\xi}^{*}(e^{-i\omega_{\xi}t} - 1)e^{i\mathbf{q}_{\parallel}\mathbf{r}_{\parallel}}. \tag{25}$$

Obviously except for a constant factor the real part of $y(\mathbf{r},t)_{T=0}$ corresponds to the relative volume change discussed above [see Eq. (18)]. However, it is the imaginary part which is responsible for the dephasing of the polarization. We will refer to $y(\mathbf{r},t)_{T=0}$ as the complex volume change, the real part being the actual relative volume change and the imaginary part, the *imaginary volume change*, being responsible for the dephasing.

III. RESULTS

A. Half-space

In this section we shall discuss the optical polarization of a QD embedded in a half-space. As in an infinite crystal[31] the excitation with an ultrashort pulse leads to the creation of a phonon occupation which separates into two parts: An occupation that remains within the QD and forms a stable polaron and a phonon wave packet, that travels into the surrounding of the QD. In an infinite crystal, once the phonon wave

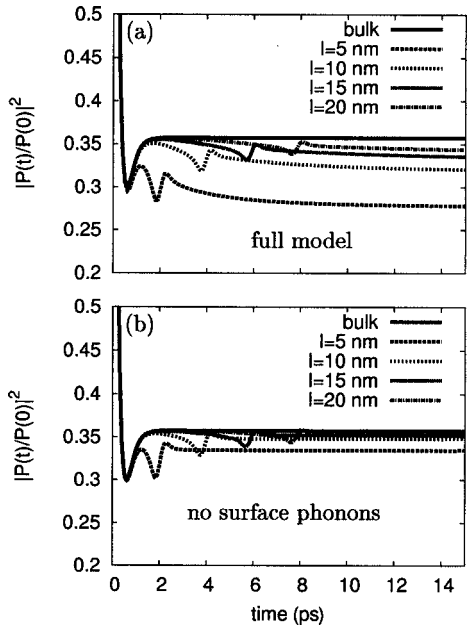

FIG. 1. Optical polarization induced by an ultrashort laser pulse at $T=4$ K. The distance l of the center of the QD from the surface is varied. The QD has a vertical size of 1.5 nm and a lateral size of 3 nm. (a) with, (b) without surface phonons.

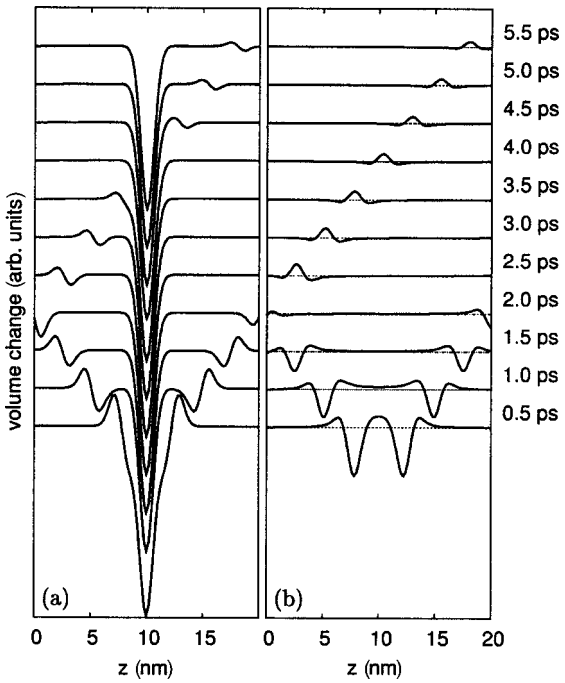

FIG. 2. Complex volume change at different times in the z direction (i.e., at $x=y=0$) for a QD located at a distance of 10 nm from the surface ($z=0$). (a) Real part, (b) imaginary part. The QD has a vertical size of 1.5 nm and a lateral size of 3 nm.

packet has left the QD, the carriers can no longer interact with it and the polarization, hence, remains at a constant value. In a half-space, however, the situation is different. The phonons traveling into the direction of the surface are reflected and those with a sufficiently small $\mathbf{q}_{\|}$ reenter the QD and allow the carriers to interact with the phonons again. We will show that this leaves a distinct trace in the polarization.

Let us consider an ellipsoidal QD with a lateral size of $L_{x,y}=3$ nm and a vertical size of $L_z=1.5$ nm. These sizes refer to the full width at half maximum of the electron charge distribution with an assumed Gaussian shape. The optical polarization for such a QD located at different distances from the surface is shown in Fig. 1(a). The solid line depicts the polarization in an infinite crystal. First, we notice that indeed for increasing distance from the surface the polarization approaches the bulk curve. Second, we observe a pronounced dip at a time which increases with increasing distance from the surface. This dip occurs roughly at a time $t=2l/c_l$, where l denotes the distance between the center of the QD and the surface, and thus corresponds to the time when the reflected wave packet returns to the dot. In addition, we can see, that the polarization in the infinite bulk system and those in a half-space are identical until $t\approx l/c_l$. At this time the emitted wave packet reaches the surface. After this a slow decay begins, which is due to the influence of the surface phonons, as can be seen from Fig. 1(b) where the same calculations have been performed, however, with the surface phonons switched off. Indeed, here the slow decay is absent.

Let us now interpret this behavior with the help of the complex volume change and concentrate on the QD located 10 nm away from the surface. Shortly after the laser pulse a relative volume change begins to build up within the QD as can be seen in Fig. 2(a), where the real volume change is plotted as a function of z at different times.[38] Part of this deformation wave travels outward in the form of a stable wave packet and the part emitted into the direction of the surface reaches it at $t\approx 1.96$ ps. Then the wave packet is reflected with a phase jump and reenters the QD at $t\approx 3.9$ ps. It then passes and leaves the QD. The reentrance of the wave packet into the QD corresponds to the dip seen in the polarization. The sharp structures in the polarization are observable exactly as long as the wave packet needs to pass the QD.

The slow decay in the polarization can be best understood with the help of the imaginary volume change shown in Fig. 2(b) which is responsible for the dephasing. When comparing the real and the imaginary volume change one sees clearly, that the imaginary volume change is broader with a long sloped shape. It is also created within the QD and travels outward, just as it would in an infinite crystal. The wave packet reaches the surface, is reflected and then travels back to the QD and through it, keeping this sloped shape.

This behavior is due to the surface phonons and is responsible for the onset of the decay already at approximately $t=2$ ps, which is only about half of the time $2l/c_l$ for the return of the reflected wave packet. The surface phonons have a displacement which is largest at the surface and decreases exponentially with increasing distance to the surface. If the QD is not too far away from the surface, part of the lattice displacement caused by the surface phonons extends into the QD and also allows carriers and phonons to interact. Since the surface phonons do not present a traveling wave in the z direction, they are restricted to progressing along the surface. The wave packet is a superposition of all phonon modes within the half-space. Therefore even directly after

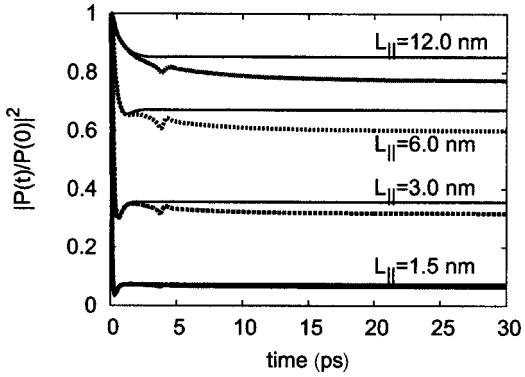

FIG. 3. Optical polarization for QDs of different lateral sizes located at a distance of 10 nm from the surface. The thin, solid lines present the polarization for the same dot size but in an infinte bulk. Vertical size: 1.5 nm.

the excitation all these modes including the surface phonons form the volume change seen in Fig. 2(b). However, only after the wave packet reaches the surface does their influence become visible. At earlier times their effect is compensated for by superpositions of the propagating modes. If the QD is located at a greater distance l from the surface the sharp structure occurs at a later time corresponding to $t \approx 2l/c_l$ and its amplitude is weaker. The weaker amplitude is due to the fact, that the initially emitted wave packet is spread over a larger space and therefore only a smaller portion of the total phonon occupation is reflected into the direction of the QD. Additionally, the strength of the slow decay is also lessened by a larger distance from the surface, since the displacement of the surface phonons and thus their influence on the QD decreases exponentially with increasing distance. While for a distance of 5 nm it leads to an additional decay of about 15%, at a distance of 20 nm this is reduced to approximately 3% of the initial polarization.

The influence of the surface phonons not only depends on the distance of the QD from the surface, but also on its lateral size as Fig. 3 shows. Here the QD is kept at a 10 nm distance, but the lateral size is varied. The vertical size remains unchanged and is given by 1.5 nm. The thin solid lines show the polarization for a QD of the same size but in the absence of a surface. For all shown QDs the sharp features occur at the same time, since the QDs size does not change the distance the wave packet has to travel from and to the QD. However the strength of the slow decay depends strongly on the size. For a spherical QD of 1.5 nm the difference between the polarization without a surface (solid line) and the polarization with a surface (dashed line) is almost undiscernable. At a lateral size of 12 nm, the difference is quite large and the contribution of the surface phonons is nearly 40% of the total dephasing. This can be easily understood, since if the QD has a greater lateral size the created surface phonons have to travel a longer distance in the x, y plane in order to leave the region where they can influence the QD.

As a last aspect of a QDs behavior in a half-space we want to study its absorption spectrum. It is easily calculated as the imaginary part of the fourier transform of the linear polarization. Figure 4 shows such spectra for a QD located at

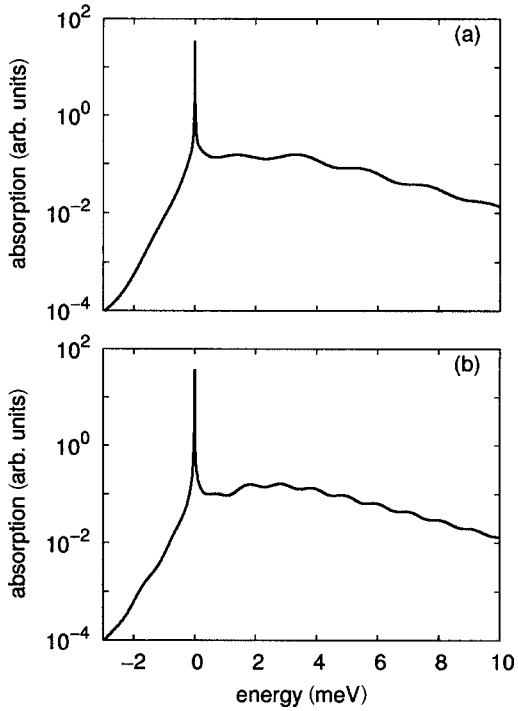

FIG. 4. Absorption spectra of QDs located at different distances from the surface, (a) 5 nm, (b) 10 nm. Temperature: T=4 K. $L_{||}$ =3 nm, L_z=1.5 nm.

the distances of 5 and 10 nm from the surface. The size of the dots was chosen as in Fig. 1. Also note, that these spectra were obtained by first multipling the polarization with a weak exponential decay $e^{-\gamma t}$ with $\gamma = 1/500\ 1/\text{ps}$ which accounts phenomenologically for the finite width of the zero-phonon line (ZPL).

The overall shape of the spectra resembles that of a QD in an infinite bulk:[37] they show a discrete ZPL as well as a broad acoustic background which is separated from the ZPL by a dip. Due to the low temperature this background is highly asymmetric. In addition to this behavior we now also see pronounced oscillations in the acoustic background, where the oscillation period and amplitude depends on the QDs distance from the surface. If this distance increases the amplitude gets weaker, so that in the limit of an infinite distance the spectrum is completely smooth. The frequency difference $\Delta\omega$ between two neighboring maxima in the spectrum is constant and corresponds to the time the wave packet requires to travel from the QD to the surface and back again.

B. Slab

In this section we shall now study the influence of the confined phonon modes in a slab on polarization and lattice displacement. Unlike in the half-space the intially emitted phonon wave packet now does not only reenter the QD once, but is reflected from both surfaces of the slab and thus passes through the QD over and over again, however, with decreasing amplitude.

Let us begin with a QD located in the center of the slab. In such a scenario the waves reflected from both sides of the

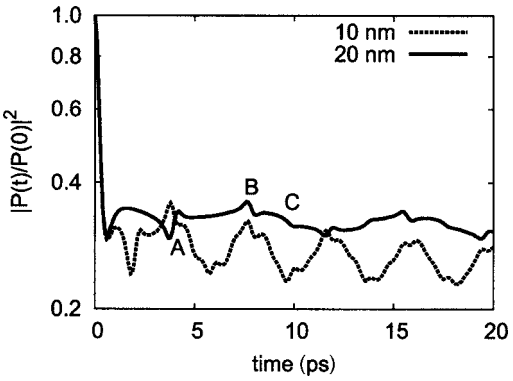

FIG. 5. Optical polarization after the excitation with an ultrashort laser pulse for a QD located in the center of a slab of 20 nm width (solid line) and in the center of a slab of 10 nm width (dashed line). Temperature: $T=4$ K. $L_{\|}=3$ nm, $L_z=1.5$ nm.

slab always reenter the QD at the same time making the fine structure of the polarization rather easy to understand.

Figure 5 shows the polarization for a QD in the center of slabs of 10 and 20 nm width. Note, that here a logarithmical scale was chosen in order to allow for a better visibility of the fine structure. First, we will analyze the polarization in the 20 nm slab. To interpret the results we will simultaneously discuss Fig. 6, which shows the relative volume change for this scenario. For the first few picoseconds the polarization looks very much like that for a QD in a half-space with a 10 nm distance to the surface (Fig. 1). The first sharp feature which in the plot is marked as *A* happens, when the reflected wave packet reenters the QD. As can be clearly seen in Fig. 6 this begins after a time $t \approx d/c_l$, where d denotes the width of the slab. Since in a slab a wave is reflected from both sides the amplitude of this oscillation is twice as large as for the similar situation in the half-space. After another d/c_l the wave has been reflected a second time and reenters the QD again. This point is marked in Fig. 5 as *B*. It is tempting to think that the second reentrance of the phonon wave packet would lead to a second sharp structure resulting in a further decrease of the polarization. However, we now find a sharp feature which first increases the polarization and then decreases it. This behavior can be understood with the help of Fig. 6. After about 6 ps the wave is reflected a second time. But since each reflection involves a phase jump, the phase of the wave is now opposite to the wave after the first reflection. Therefore, the reentering waves alternatingly lead to structures with opposite phases. This prevents the polarization from being destroyed step by step as each wave packet reenters the QD. As can be seen when comparing both polarizations in Fig. 5, the periodicity of these repeating structures depends on the slab width. With progressing time, the amplitude of this large oscillation becomes weaker, so that the polarization remains at a finite value which after a long time is asymptotically constant.

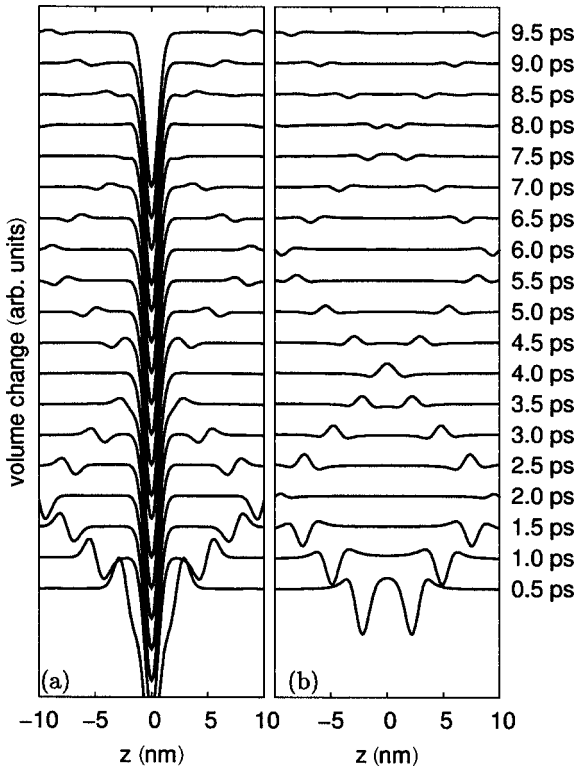

FIG. 6. Relative (a) and imaginary volume change (b) for a QD located in a slab of 20 nm width.

Let us return to the case $d=20$ nm. Until now we have only accounted for the longitudinal phonons, which are not converted during the reflection process. However, as discussed in Sec. II, during each reflection longitudinal waves are partially converted to transverse waves and (after the first reflection) vice versa. The transverse waves created in the first reflection do not cause a relative volume change, but nevertheless they can be seen in Fig. 6 indirectly. During the second reflection these transverse phonons are in part reconverted into longitudinal phonons, which do cause a relative volume change. Since the sound velocity of transverse phonons is smaller than that of longitudinal ones, they reach the surface later than the longitudinal ones. Therefore, after the longitudinal phonons have been reflected for a second time, a second wave packet can be seen in the relative volume change. It is rather weak, but can be discerned in Fig. 6 at $t=8$ ps in the dip of the relative volume change close to the surfaces and again at $t=8.5$ ps, where it has traveled approximately 4 nm into the direction of the QD. This packet reenters the QD after 9.8 ps and is therefore responsible for the dip marked as *C* in Fig. 5. In the following reflections these conversions occur again and again creating more and more separate wave packets that reach the QD at different times. Therefore, after *C*, the fine structure of the polarization becomes more complicated and after some time the separate dips are blurred.

Let us now take a look at QDs that are located at different positions within the slab. Figure 7 shows the polarization for a QD in a slab of 40 nm width at different positions within the slab. Here a stands for the QDs displacement from the center of the slab. One can see clearly, that now the sharp features occur at quite different times, depending on the distance which the wave packets have to travel. For the two QDs in the plot, that are not located in the middle of the slab, the first reentrance of the phonon wave packets initially emitted into opposite directions does not occur at the same time. One can now differentiate between two oscillations in the

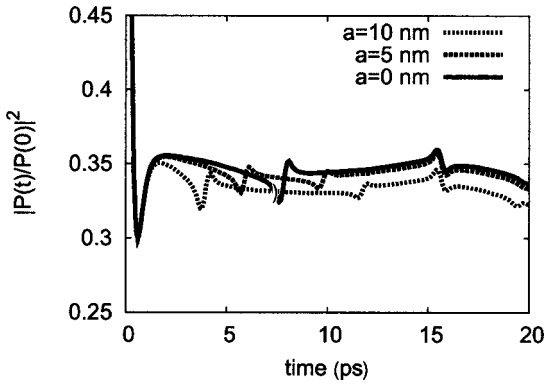

FIG. 7. Optical polarization after an excitation with an ultrashort laser pulse and for a temperature of 4 K for QDs located at different positions within a slab of 40 nm width.

polarization, which both show the characteristics of the first reenterance (first a dip, then a peak). With decreasing a these two oscillations move closer together in time and are united for the case $a=0$ nm. However, all wave packets reenter the QD for a second time after about 15 ps, when they have passed the slab twice, regardless of their starting point. This very pronounced oscillation therefore shows the characteristics of the second reenterance (first a peak, then a dip).

As a last result let us take a look at the absorption spectra of QDs located in the middle of a slab calculated at a temperature of 4 K. Figure 8 shows spectra for two slab widths: 20 and 40 nm. The corresponding polarizations can be seen in Figs. 5 and 7.

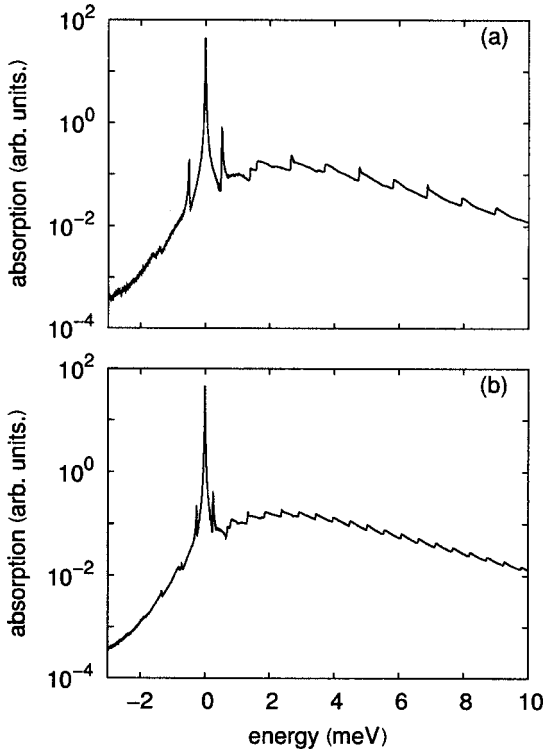

FIG. 8. Absorption spectra of QDs located in the middle of two different slabs, (a) $d=20$ nm, (b) $d=40$ nm. Temperature: $T=4$ K. $L_{\|}=3$ nm, $L_z=1.5$ nm. The polarizations were multiplied with an exponential decay with $\gamma=1/100$ 1/ps.

Again, the overall shape of the spectra resembles those in an infinite bulk, but is superposed by a complex fine structure. Especially striking are two strong peaks located at the same distance to the left and right of the ZPL. These peaks can be interpreted as van Hove singularities. For a slab with $d=20$ nm they are found at energies $\hbar 0.8\ 1/ps$ from the ZPL. This corresponds to a minimum in the dispersion relation $\omega_{q_{\|},q_l,\mathrm{dil}}$ for a finite $q_{\|}$, which is therefore connected with an infinite density of states. Note, that since here the QD is located in the center of the slab only the phonon frequencies of the dilatational modes are of importance. For increasing slab width this minimum in the dispersion relation is found at lower frequencies, so that these peaks are closer to the ZPL for the larger slab in Fig. 8(b). Evidence for this van Hove singularity has also been found in the study of transport properties of a double quantum dot embedded in a slab:[23,24] the phonon emission rates showed a related effect. The frequencies of the singularities found in Ref. 23 agree very well with those presented here.

In addition the spectra show steplike features, which can be explained with the structure of the dispersion relation. The phonon frequencies $\omega_{q_{\|},q_l,\mathrm{dil}}$ can be regarded as separated into subbands for the different discrete values of q_l. Each step in the absorption spectrum corresponds to the onset of a phonon subband.

IV. CONCLUSION

In this paper we have analyzed the optical polarization induced by an ultrashort laser pulse and the resulting relative volume change of the surrounding lattice for QDs located in half-space and free-standing slabs. It was shown that the proximity of the QD to a surface results in distinct signatures in the optical polarization which cannot be found in situations where the QD is located in an infinite bulk. In a half-space the initially emitted phonon wave packet, when reentering the QD, leads to a sharp feature in the polarization and the involved surface phonons induce an additional decay. Depending on the vicinity of the QD to the surface and the size of the QD parallel to the surface, these surface phonons can induce an additional decay of up to several tens of percents of the decay in the absence of a surface. In a slab, the decay is not increased step by step with each reentrance of the phonons into the QD, as could be expected. Rather, the phase jump in the reflection of the phonon wave packet leads to an oscillatory behavior, so that the polarization remains at a finite value at all times as in the case of dots in an infinite bulk system. Interestingly, in the case of a slab also the transverse phonons leave a weak but clearly visible trace in the optical polarization although they do not couple directly to the electrons and holes. The reason is that they can be created by mode conversion during a reflection process and at the next reflection they can be converted back to longitudinal waves which again couple to the QD states.

A common feature of both geometries investigated is the fact that we find structures in the time-dependent polarization or, equivalently, in the absorption spectra which are directly related to the time a longitudinal acoustic phonon needs to travel from the QD to the surface and back to the

QD. If the distance of the QD from the surface is known, this is a well known value. Therefore it should be easily possible to separate the phenomena studied here from other phenomena like, e.g., a partial phonon confinement in the QD or surface-related features which are not associated with phonons.

ACKNOWLEDGMENT

This work has been partially supported by the Deutsche Forschungsgemeinschaft within the *Graduiertenkolleg Nichtlineare kontinuierliche Systeme*.

APPENDIX A: DEFORMATION POTENTIAL COUPLING IN A HALF-SPACE

1. Dilatational and Flexural Modes

The coupling matrix element for the dilatational modes is given by

$$\mathcal{G}^c_{q_\parallel,q_l,\mathrm{dil}} = -\frac{D^c}{2\pi}\sqrt{\frac{1}{2\varrho\hbar\omega_{q_\parallel,q_l,\mathrm{dil}}}}N_{\mathrm{dil}}2q_\parallel^2 q_t(q_\parallel^2+q_l^2) \quad \text{(A1)}$$

with the normalization factor

$$|N_{\mathrm{dil}}|^2 = \frac{q_l}{2\pi}\left\{q_\parallel^2 q_t(q_\parallel^2+q_l^2)\left[q_\parallel^2 q_t q_l + \frac{1}{4}(q_\parallel^2-q_t^2)^2\right]\right\}^{-1} \quad \text{(A2)}$$

and the form factor

$$\mathcal{F}^c_{q_\parallel,q_l,\mathrm{dil}} = \int_{HS}|\varphi^c(\mathbf{r})|^2 e^{i\mathbf{q}_\parallel\mathbf{r}_\parallel}\cos q_l z\, d^3r. \quad \text{(A3)}$$

Here the integration runs over the complete half-space denoted by HS. The coupling matrix element for the flexural modes is

$$\mathcal{G}^c_{q_\parallel,q_l,\mathrm{flex}} = -\frac{D^c}{2\pi}\sqrt{\frac{1}{2\varrho\hbar\omega_{q_\parallel,q_l,\mathrm{flex}}}}N_{\mathrm{flex}}2(q_\parallel^2-q_t^2)q_t(q_\parallel^2+q_l^2) \quad \text{(A4)}$$

with the normalization factor

$$|N_{\mathrm{flex}}|^2 = \frac{1}{2\pi}\left\{q_t^2(q_\parallel^2+q_l^2)\left[q_\parallel^2 q_t q_l + \frac{1}{4}(q_\parallel^2-q_t^2)^2\right]\right\}^{-1} \quad \text{(A5)}$$

and the form factor

$$\mathcal{F}^c_{q_\parallel,q_l,\mathrm{flex}} = \int_{HS}|\varphi^c(\mathbf{r})|^2 e^{i\mathbf{q}_\parallel\mathbf{r}_\parallel}\sin q_l z\, d^3r. \quad \text{(A6)}$$

2. Mixed Modes

The coupling matrix element for the mixed modes is given by

$$\mathcal{G}^c_{q_\parallel,q_l,\mathrm{mix}} = \frac{D^c}{2\pi}\sqrt{\frac{1}{2\varrho\hbar\omega_{q_\parallel,q_l,\mathrm{mix}}}}N_{\mathrm{mix}}2q_\parallel^2 q_t(q_t^2-q_\parallel^2)(q_l^2-q_\parallel^2) \quad \text{(A7)}$$

with the normalization factor

$$|N_{\mathrm{mix}}|^2 = \frac{q_l}{2\pi}\left\{(q_\parallel^2-q_l^2)q_\parallel^2 q_t\left[4q_\parallel^4 q_t^2 q_l^2 + \frac{1}{4}(q_t^2-q_\parallel^2)^4\right]\right\}^{-1} \quad \text{(A8)}$$

and the form factor

$$\mathcal{F}^c_{q_\parallel,q_l,\mathrm{mix}} = \int_{HS}|\varphi^c(\mathbf{r})|^2 e^{i\mathbf{q}_\parallel\mathbf{r}_\parallel}e^{-q_l z}d^3r. \quad \text{(A9)}$$

3. Rayleigh Modes

The coupling matrix element for the surface modes is given by

$$\mathcal{G}^c_{q_\parallel,q_l,\mathrm{sur}} = \frac{D^c}{2\pi}\sqrt{\frac{1}{2\varrho\hbar\omega_{q_\parallel,q_l,\mathrm{sur}}}}N_{\mathrm{sur}}(q_\parallel^2+q_t^2)(q_\parallel^2-q_l^2) \quad \text{(A10)}$$

with

$$|N_{\mathrm{sur}}|^2 = \left[\frac{1}{2q_l}(q_\parallel^2+q_t^2)^2(q_\parallel^2+q_l^2) + 4\frac{1}{2q_t}q_\parallel^2 q_l^2(q_\parallel^2+q_t^2) - 4(q_\parallel^2+q_t^2)q_\parallel^2 q_l\right]^{-1} \quad \text{(A11)}$$

and

$$\mathcal{F}^c_{q_\parallel,q_l,\mathrm{sur}} = \int_{HS}|\varphi^c(\mathbf{r})|^2 e^{i\mathbf{q}_\parallel\mathbf{r}_\parallel}e^{-q_l z}d^3r. \quad \text{(A12)}$$

APPENDIX B: DEFORMATION POTENTIAL COUPLING IN A SLAB

In the case of a slab q_l and q_t can be either both real, both purely imaginary or q_t can be real and q_l purely imaginary.

1. Dilatational Modes

The coupling matrix element for the dilatational modes in slab geometry is given by

$$\mathcal{G}^c_{q_\parallel,q_l,\mathrm{dil}} = \frac{D^c}{2\pi}\sqrt{\frac{1}{2\varrho\hbar\omega_{q_\parallel,q_l,\mathrm{dil}}}}F_{\mathrm{dil}}(q_t^2-q_\parallel^2)(q_l^2+q_\parallel^2)\sin\frac{dq_t}{2} \quad \text{(B1)}$$

with the form factor

$$\mathcal{F}^c_{q_\parallel,q_l,\mathrm{dil}} = \int_{\mathrm{slab}}|\varphi^c(\mathbf{r})|^2 e^{i\mathbf{q}_\parallel\mathbf{r}_\parallel}\cos q_l z\, d^3r. \quad \text{(B2)}$$

If q_l and q_t are both real or both purely imaginary, the normalization factor reads[20]

$$F_{\mathrm{dil}}^{-2}=\frac{1}{8q_lq_t}[2dq_l^3q_t^5+4dq_l^3q_t^3q_\parallel^2+2dq_lq_t^5q_\parallel^2+10dq_l^3q_tq_\parallel^4 - 4dq_lq_t^3q_\parallel^4+2dq_lq_tq_\parallel^6-8dq_l^3q_tq_\parallel^2(q_t^2+q_\parallel^2)\cos dq_l - 2dq_lq_t(q_t^2-q_\parallel^2)^2(q_l^2+q_\parallel^2)\cos dq_t+2q_t(-q_t^2+q_\parallel^2)(q_l^2q_t^2 + 7q_l^2q_\parallel^2-q_t^2q_\parallel^2+q_\parallel^4)\sin dq_l+8q_l^3q_\parallel^2(q_t^2-q_\parallel^2)\sin dq_t + (q_l^2q_t^5+4q_l^3q_t^2q_\parallel^2+6q_l^2q_t^3q_\parallel^2-q_t^5q_\parallel^2-4q_l^3q_\parallel^4-7q_l^2q_tq_\parallel^4 + 2q_t^3q_\parallel^4-q_tq_\parallel^6)\sin d(q_l-q_t)+(q_l^2q_t^5-4q_l^3q_t^2q_\parallel^2 + 6q_l^2q_t^3q_\parallel^2-q_t^5q_\parallel^2+4q_l^3q_\parallel^4-7q_l^2q_tq_\parallel^4+2q_t^3q_\parallel^4 - q_tq_\parallel^6)\sin d(q_l+q_t)], \tag{B3}$$

and if q_t is real and $q_l=ip_l$ is purely imaginary, then we have

$$F_{\mathrm{dil}}^{-2}=\frac{1}{4p_lq_t}[-dp_l^3q_t^5-2dp_l^3q_t^3q_\parallel^2+dp_lq_t^5q_\parallel^2-5dp_l^3q_tq_\parallel^4 - 2dp_lq_t^3q_\parallel^4+dp_lq_tq_\parallel^6+4dp_l^3q_tq_\parallel^2(q_t^2+q_\parallel^2)\cosh dp_l + dp_lq_t(p_l^2-q_\parallel^2)(q_t^2-q_\parallel^2)^2\cos dq_t+(p_l^2q_t^5+6p_l^2q_t^3q_\parallel^2 + q_t^5q_\parallel^2-7p_l^2q_tq_\parallel^4-2q_t^3q_\parallel^4+q_tq_\parallel^6)\sinh dp_l+4p_l^3q_\parallel^2(-q_t^2 + q_\parallel^2)\sin dq_t-4p_l^3q_\parallel^2(q_\parallel^2-q_t^2)\cosh dp_l\sin dq_t+(-p_l^2q_t^5 - 6p_l^2q_t^3q_\parallel^2-q_t^5q_\parallel^2+7p_l^2q_tq_\parallel^4+2q_t^3q_\parallel^4 - q_tq_\parallel^6)\sinh dp_l\cos dq_t]. \tag{B4}$$

2. Flexural Modes

The coupling matrix element involving the flexural modes is given by

$$\mathcal{G}^c_{q_\parallel,q_l,\mathrm{flex}}=\frac{D^c}{2\pi}\sqrt{\frac{1}{2\varrho\hbar\omega_{q_\parallel,q_l,\mathrm{flex}}}}F_{\mathrm{flex}}(q_t^2-q_\parallel^2)(q_l^2+q_\parallel^2)\cos\frac{dq_t}{2} \tag{B5}$$

with the form factor

$$\mathcal{F}^c_{q_\parallel,q_l,\mathrm{flex}}=\int_{\mathrm{slab}}|\varphi^c(\mathbf{r})|^2e^{i\mathbf{q}_\parallel\mathbf{r}_\parallel}\sin q_lz\,d^3r. \tag{B6}$$

If q_l and q_t are both real or both purely imaginary, the normalization factor for the flexural modes is[20]

$$F_{\mathrm{flex}}^{-2}=\frac{1}{8q_lq_t}[2dq_l^3q_t^5+4dq_l^3q_t^3q_\parallel^2+2dq_lq_t^5q_\parallel^2+10dq_l^3q_tq_\parallel^4 - 4dq_lq_t^3q_\parallel^4+2dq_lq_tq_\parallel^6+8dq_l^3q_tq_\parallel^2(q_t^2+q_\parallel^2)\cos dq_l + 2dq_lq_t(q_t^2-q_\parallel^2)^2(q_l^2+q_\parallel^2)\cos dq_t+2q_t(q_t^2-q_\parallel^2)(q_l^2q_t^2 + 7q_l^2q_\parallel^2-q_t^2q_\parallel^2+q_\parallel^4)\sin dq_l+8q_l^3q_\parallel^2(-q_t^2+q_\parallel^2)\sin dq_t + (q_l^2q_t^5+4q_l^3q_t^2q_\parallel^2+6q_l^2q_t^3q_\parallel^2-q_t^5q_\parallel^2-4q_l^3q_\parallel^4-7q_l^2q_tq_\parallel^4 + 2q_t^3q_\parallel^4-q_tq_\parallel^6)\sin d(q_l-q_t)+(q_l^2q_t^5-4q_l^3q_t^2q_\parallel^2 + 6q_l^2q_t^3q_\parallel^2-q_t^5q_\parallel^2+4q_l^3q_\parallel^4-7q_l^2q_tq_\parallel^4+2q_t^3q_\parallel^4 - q_tq_\parallel^6)\sin d(q_l+q_t)] \tag{B7}$$

and if q_t is real and $q_l=ip_l$ is purely imaginary, then we have

$$F_{\mathrm{flex}}^{-2}=\frac{1}{4p_lq_t}[dp_l^3q_t^5+2dp_l^3q_t^3q_\parallel^2-dp_lq_t^5q_\parallel^2+5dp_l^3q_tq_\parallel^4 + 2dp_lq_t^3q_\parallel^4-dp_lq_tq_\parallel^6+4dp_l^3q_tq_\parallel^2(q_t^2+q_\parallel^2)\cosh dp_l + dp_lq_t(p_l^2-q_\parallel^2)(q_t^2-q_\parallel^2)^2\cos dq_t+(p_l^2q_t^5+6p_l^2q_t^3q_\parallel^2 + q_t^5q_\parallel^2-7p_l^2q_tq_\parallel^4-2q_t^3q_\parallel^4+q_tq_\parallel^6)\sinh dp_l+4p_l^3q_\parallel^2(q_\parallel^2 - q_t^2)\sin dq_t+4p_l^3q_\parallel^2(q_\parallel^2-q_t^2)\cosh dp_l\sin dq_t+(p_l^2q_t^5 + 6qp_l^2q_t^3q_\parallel^2+q_t^5q_\parallel^2-7p_l^2q_tq_\parallel^4-2q_t^3q_\parallel^4 + q_tq_\parallel^6)\sinh dp_l\cos dq_t]. \tag{B8}$$

*Email address: krummheu@nwz.uni-muenster.de

[1] D. Bimberg, M. Grundmann, and N. N. Ledentsov, *Quantum Dot Heterostructures* (Wiley, Chichester, 1999).

[2] P. Michler, A. Kiraz, C. Becher, W. V. Schoenfeld, P. M. Petroff, L. Zhang, and A. Imamoglu, Science **290**, 2282 (2000).

[3] A. Barenco, D. Deutsch, A. Ekert, and R. Jozsa, Phys. Rev. Lett. **74**, 4083 (1995); E. Biolatti, R. C. Iotti, P. Zanardi, and F. Rossi, *ibid.* **85**, 5647 (2000); T. Amand, X. Marie, M. Sénès, O. Krebs, S. Laurent, S. Cortez, P. Voisin, and J. M. Gérard, Superlattices Microstruct. **32**, 157 (2002); E. Pazy, E. Biolatti, T. Calarco, I. D'Amico, P. Zanardi, F. Rossi, and P. Zoller, Europhys. Lett. **62**, 175 (2003); F. Troiani, E. Molinari, and U. Hohenester, Phys. Rev. Lett. **90**, 206802 (2003).

[4] T. R. Meeker, A. H. Meitzler, in *Physical Acoustics*, edited by W. P. Warren (Academic Press, New York, 1964) Vol. I, Part A.

[5] A. Sommerfeld, *Mechanik der Deformierbaren Körper* (Akademische Verlagsgesellschaft Geest & Portig K.-G., Leipzig, 1964); English edition: A. Sommerfeld, *Mechanics of Deformable Bodies* (Academic Press, New York, 1950).

[6] H. Ezawa, Ann. Phys. **67**, 438 (1971).

[7] L. Wendler and V. G. Grigorian, Surf. Sci. **206**, 203 (1988).

[8] K. W. Kim and M. A. Stroscio, J. Appl. Phys. **68**, 6289 (1990).

[9] G. Q. Hai, F. M. Peeters, and J. T. Devreese, Phys. Rev. B **48**, 4666 (1993).

[10] B. C. Lee, K. W. Kim, M. A. Stroscio, and M. Dutta, Phys. Rev. B **58**, 4860 (1998).

[11] S. M. Komirenko, K. W. Kim, M. A. Stroscio, and M. Dutta, Phys. Rev. B **59** 5013 (1999).

[12] D. V. Melnikov and W. B. Fowler, Phys. Rev. B **64**, 245320 (2001).

[13] L. Zhang, H.-J. Xie, and C.-Y. Chen, Phys. Rev. B **66**, 205326 (2002).

[14] B. El Amrani, M. Fliyou, L. Bensaid, T. Lamcharfi, K. Rahmani, and M. Bouayad, J. Appl. Phys. **94**, 437 (2003).

[15] O. Reese, L. C. Lew Yan Voon, and M. Willatzen, Phys. Rev. B **70**, 075401 (2004).
[16] P. Bordone and P. Lugli, Phys. Rev. B **49**, 8178 (1994).
[17] Y. M. Sirenko, K. W. Kim, and M. A. Stroscio, Phys. Rev. B **56**, 15770 (1997).
[18] V. I. Pipa, N. Z. Vagidov, V. V. Mitin, and M. Stroscio, Physica B **270**, 280 (1999).
[19] M. A. Stroscio and K. W. Kim, Phys. Rev. B **48**, 1936 (1993).
[20] N. Bannov, V. Mitin, and M. Stroscio, Phys. Status Solidi B **183**, 131 (1994).
[21] N. Bannov, V. Aristov, V. Mitin, and M. A. Stroscio, Phys. Rev. B **51**, 9930 (1995).
[22] B. A. Glavin, V. I. Pipa, V. V. Mitin, and M. A. Stroscio, Phys. Rev. B **65**, 205315 (2002).
[23] S. Debald, T. Brandes, and B. Kramer, Phys. Rev. B **66**, 041301(R) (2002).
[24] T. Brandes, Phys. Rep. **408**, 315 (2005).
[25] S. Rufo, M. Dutta, and M. A. Stroscio, J. Appl. Phys. **93**, 2900 (2003).
[26] E. M. Weig, R. H. Blick, T. Brandes, J. Kirschbaum, W. Wegscheider, M. Bichler, and J. P. Kotthaus, Phys. Rev. Lett. **92**, 046804 (2004).
[27] E. M. Höhberger, J. Kirschbaum, R. H. Blick, J. P. Kotthaus, and W. Wegscheider, Physica E (Amsterdam) **18**, 99 (2003).
[28] T. Takagahara, Phys. Rev. B **60**, 2638 (1999).
[29] P. Palinginis and H. Wang, Appl. Phys. Lett. **78**, 1541 (2001).
[30] A. Vagov, V. M. Axt, T. Kuhn, W. Langbein, P. Borri, and U. Woggon, Phys. Rev. B **70**, 201305(R) (2004).
[31] A. Vagov, V. M. Axt, and T. Kuhn, Phys. Rev. B **66**, 165312 (2002).
[32] B. Krummheuer, V. M. Axt, T. Kuhn, I. D'Amico, and F. Rossi, Phys. Rev. B **71**, 235329 (2005).
[33] M. A. Stroscio and M. Dutta, *Phonons in Nanostructures* (Cambridge University Press, Cambridge, 2001).
[34] B. A. Auld, *Acoustic Waves and Fields in Solids* (Wiley, New York, 1973), Vol. II.
[35] O. Madelung, *Introduction to Solid-State Theory* (Springer-Verlag, Berlin, 1978).
[36] A. Vagov, V. M. Axt, and T. Kuhn, Physica E (Amsterdam) **17**, 11 (2003).
[37] B. Krummheuer, V. M. Axt, and T. Kuhn, Phys. Rev. B **65**, 195313 (2002).
[38] Note, that while the polarizations and spectra presented in this paper are calculated at a realistic temperature of $T=4$ K, the volume change is given at $T=0$ K. This allows for a clearer definition of the real and imaginary volume change as shown in Sec. II C and the difference between the volume change at these two temperatures is negligible.